

Self-Powered Tactile Sensor with Learning and Memory

Chaoxing Wu,^{†,||} Tae Whan Kim,^{*,†,||} Jae Hyeon Park,[†] Bonmin Koo,[†] Sihyun Sung,[†] Jiajia Shao,[‡] Chi Zhang,^{‡,||} and Zhong Lin Wang^{*,†,§,||}

[†]Department of Electronic and Computer Engineering, Hanyang University, Seoul 04763, Republic of Korea

[‡]Beijing Institute of Nanoenergy and Nanosystems, Chinese Academy of Sciences, and National Center for Nanoscience and Technology (NCNST), Beijing 100083, People's Republic of China

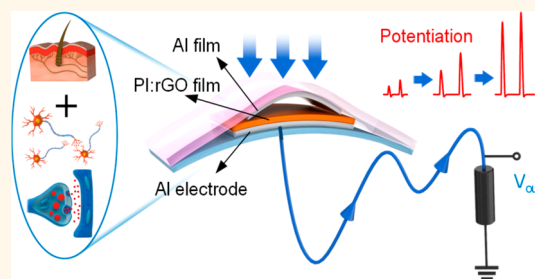
[§]School of Materials Science and Engineering, Georgia Institute of Technology, Atlanta, Georgia 30332, United States of America

^{||}College of Physics and Information Engineering, Fuzhou University, Fuzhou, 35000, PR China

Supporting Information

ABSTRACT: Fabrication of human-like intelligent tactile sensors is an intriguing challenge for developing human–machine interfaces. As inspired by somatosensory signal generation and neuroplasticity-based signal processing, intelligent neuromorphic tactile sensors with learning and memory based on the principle of a triboelectric nanogenerator are demonstrated. The tactile sensors can actively produce signals with various amplitudes on the basis of the history of pressure stimulations because of their capacity to mimic neuromorphic functions of synaptic potentiation and memory. The time over which these tactile sensors can retain the memorized information is alterable, enabling cascaded devices to have a multilevel forgetting process and to memorize a rich amount of information. Furthermore, smart fingers by using the tactile sensors are constructed to record a rich amount of information related to the fingers' current actions and previous actions. This intelligent active tactile sensor can be used as a functional element for artificial intelligence.

KEYWORDS: intelligent tactile sensor, neuroplasticity, learning, memory, triboelectric nanogenerator, graphene



Electronic sensors that are able to emulate biological sensory-perception systems are highly attractive due to the intense worldwide interests in artificial intelligence.^{1–3} Because tactile sense undertakes the majority of information perceived for learning and memory, electronic tactile sensors mimicking mechanoreceptors have been intensively studied.^{4–7} Current electronic tactile sensors have several interesting features, such as mechanical flexibility, device scalability, and fundamental interfacial mechanics and chemistries.^{8–11} Especially, in efforts to limit power consumption, nanogenerator-based self-powered techniques having been emerging as a focus in research with applications to widely distributed tactile sensors.^{12–15} However, the currently developed electronic tactile sensors mostly have a single function, which is the simple transduction of external pressure into electrical signals, so they cannot meet the demand for intelligent information preprocessing when applied in artificial intelligent systems. Therefore, the development of an electronic tactile sensor, such as a human mechanoreceptor system, that can communicate with nerve centers to realize “intelligent” sensing is still an intriguing challenge and remains an open area in research on electronic tactile sensors.

Biologically, afferent neurons transmit messages received from mechanoreceptors to the somatosensory cortex, and the human brain processes these multidimensional signals through an energy-efficient and fault-tolerant computation process (Figure 1a).¹⁶ Thus, humans tend to remember frequent mechanical stimulations and establish a sensory memory, short-term memory (STM), and long-term memory (LTM), as well as reflexes responding to these stimulations.¹⁷ Neuroplasticity, the ability of the brain to change throughout an individual's life, plays a key role in information processes,¹⁸ which has driven the emergence of neuromorphic circuits, including artificial synapses, artificial neurons, and artificial neural networks.^{19–28} Particularly, an artificial nociceptor based on a diffusive memristor can functionally mimic the intelligent communication between a human nociceptor and nerve centers, including “threshold”, “relaxation”, “no adaptation”, “sensitization”, and “cure”.²⁹ Additionally, electrical connections between tactile sensors and neuromorphic

Received: September 10, 2019

Accepted: November 20, 2019

Published: November 20, 2019

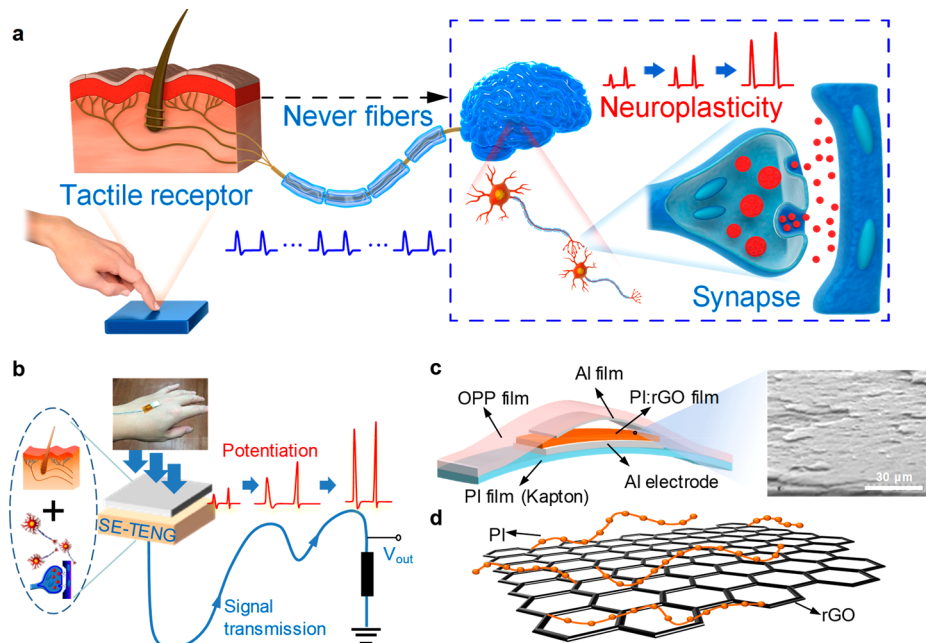


Figure 1. Artificial tactile sensor in comparison with a tactile receptor and the related afferent nerve system. (a) Schematic of a tactile receptor and the related afferent nerve system. Pressures applied to mechanoreceptors change the receptor potential of each mechanoreceptor. The afferent neurons transmit messages received from the mechanoreceptors to the human brain to process these multidimensional signals. The neuroplasticity in the human cerebral cortex plays a key role in the information process. (b) The intelligent neuromorphic sensor based on SE-TENG technology can functionally emulate combined mechanoreceptor and neuromorphic systems. (c) Schematic of the intelligent neuromorphic sensor and SEM image of the PI:rGO film. (d) Schematic structure of the PI:rGO nanocomposites.

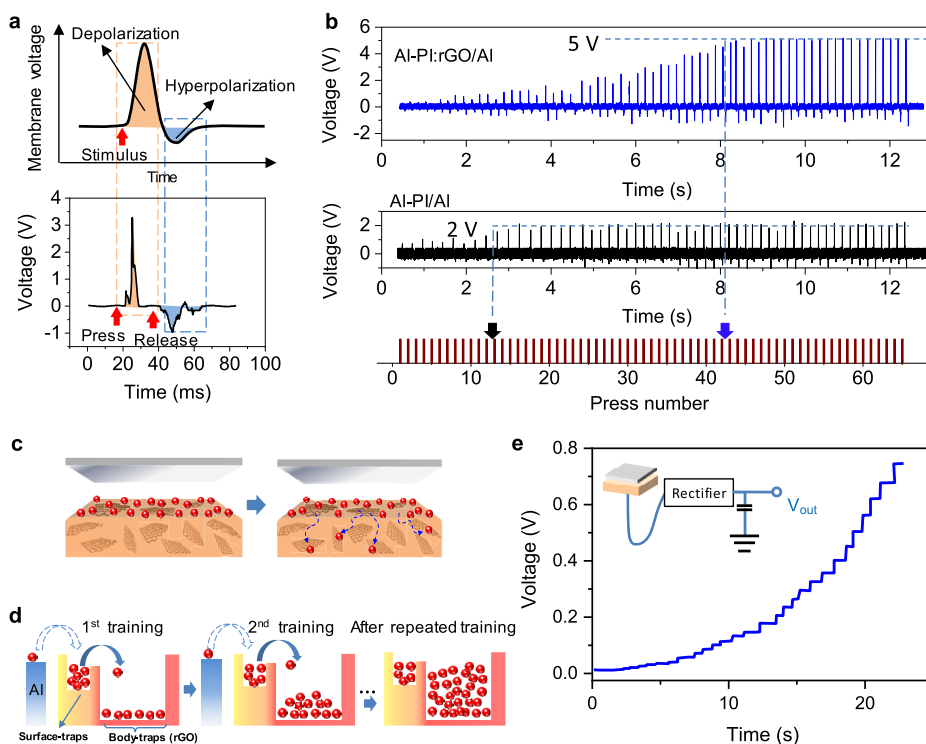


Figure 2. Electrical performances and operation mechanism. (a) Output signal of the intelligent neuromorphic sensor during a single press-release process and schematic of a biological action potential. The waveform of the generated voltage is similar to the biological action potential (top panel). (b) Output voltages of the Al-PI:rGO/Al and the Al-PI/Al devices, respectively. (c) Schematic process showing the triboelectric electrons transferring from the surface of the PI:rGO to the rGO sheet. (d) Schematic process showing the triboelectric electrons transferring from the surface traps to the body traps. (e) Charging process by using a capacitor as the load device. Inset is the schematic diagram of the system.

devices have also been proposed for mimicking intelligent sensing.^{1,30,31} However, the integration level of the intelligent sensor network would be limited because the sensors and the neuromorphic devices are spatially separate. Furthermore, an external power source is necessary to drive the connected sensor and neuromorphic devices, which would increase power consumption of the system.

Functionally inspired by somatosensory signal generation and neuroplasticity-based signal processes, we demonstrate a self-powered intelligent tactile sensor with learning ability and alterable memory. The configuration of our device is ultrasimple, consisting of a well-designed single-electrode-based triboelectric nanogenerator (SE-TENG) (Figure 1b). Because of the utilization of nanogenerator technology,^{32–34} the device can actively produce pressure-triggered electric signals without the need for an external power supply. Furthermore, reduced graphene oxides (rGOs) embedded in the friction layer are employed to act as electron-body traps to obtain neuroplasticity. Thus, a combined mechanoreceptor and neuromorphic system can be functionally emulated without the need for separate neuromorphic circuits.^{1,30,31} Signals with various amplitudes are generated on the basis of the history of previous stimulations, and the sensor can intelligently record two-dimensional information, including current and previous stimulation information.

RESULTS AND DISCUSSION

A schematic structure of the intelligent neuromorphic sensor is shown in Figure 1c. The key component is the well-designed negative triboelectric layer: the polyimide:reduced graphene oxide (PI:rGO) hybrid layer (Figure 1d, Figures S1 and S2). The working principle of the SE-TENG is the same as that reported for a TENG (Figure S3).³⁵ Due to the employment of TENG technology, our intelligent neuromorphic sensor can actively generate voltage pulses under mechanical pressure. It means our intelligent neuromorphic sensor can actively produce action potentials similar to the biological action potentials generated by mechanoreceptors. The press-release cycle produces a voltage signal with a positive component followed by a negative component (Figure 2a, bottom). The generated voltage waveform is, to some degree, similar to the biological action potential (Figure 2a, top).³⁶ It should be noted that during the vertical contact–separation process, the duration time Δt of the separation (release) process is longer than that of the vertical contact (pressure holding) process due to the use of the arch-shaped structure.³⁷ The voltage (V) across the resistor (R) can be calculated as

$$V = I \cdot R = \frac{\Delta Q}{\Delta t} \cdot R \quad (1)$$

The total charge (ΔQ) flowing through the load resistor in the positive direction should be identical to that flowing through the resistor in the negative direction. Thus, because Δt is smaller, the positive-polarity voltage across the resistor is higher than the negative one.

The significant feature of the intelligent neuromorphic sensor is its remarkable output, which increases with increasing number of presses (Figure 2b). If not otherwise specified in the following discussion, the applied pressure is 400 Pa, the pressure holding time is 0.05 s, and the time intervals between two successive pressure applications is 0.2 s. For the fresh device, the first press leads to a low output (0.3 V). As the number of presses is increased, the output monotonically

increases and finally reaches a saturated value of ~ 5 V after the 42nd press (Figure 2b, top); moreover, the device has reliable durability as shown in Figure S4. For the device with only a pure PI layer, a similar phenomenon of increasing output with increasing press number is also observed (Figure 2b, middle). However, the final output value is much lower, and the output voltage reaches its saturated value faster.

Of note is that the output voltage is proportional to the density of the electrons transferred during the triboelectrification process.³³ The increasing output shown by the Al–PI/Al device is a common phenomenon in TENG-based devices due to the rough surfaces of the triboelectric layers and the noncomplete contact between those layers. With increasing number of contact/release cycles, the static electrons increasingly accumulate on the PI surface, and the output voltage increases accordingly (Figure S5). According to the surface-states model, when a metal is in contact with a dielectric, those electrons with high energy in the metal hop into the surface states of the dielectric. Thus, we can refer to these surface states as surface traps for static electrons. Because the total number of surface traps in the PI layer is limited, the final saturated electron density is only slightly higher than that in the initial state, as schematically demonstrated in Figure S6.

For the device with rGO, the rGO sheets can act as electron traps in the PI layer to promote the charge transfer process from PI to rGO sheets.³⁸ Thus, the triboelectric electrons on the surface (surface traps) of the PI:rGO hybrid layer spontaneously transfer to the rGO sheets (body traps) (Figure 2c). In the first contact–separation cycle (first training), when the Al film is in contact with the PI:rGO layer, electrons in the Al film hop up into the surface traps of the PI:rGO layer. Then, the occupied energy levels in the surface trap increase to the Fermi level of Al, and the triboelectrification process stops.^{39–42} After the separation of the Al film from the PI:rGO layer, most electrons in the surface traps will subsequently transfer to the body traps.³⁸ Finally, the occupied energy levels in the surface traps will decrease almost to the energy levels of the initial state. In the second training, a similar transfer of electrons from the Al layer to the PI:rGO layer occurs and the electrons in the surface traps subsequently transfer to the body traps again. As a result, the total number of generated triboelectric electrons increases, and the output voltage is definitely higher than the initial output voltage. After enough training, the triboelectric electrons captured in the PI:rGO layer reach a maximum, and the output voltage becomes saturated (Figure 2d).

When using a capacitor as the load device, voltage across the capacitor can directly reflect the charge quantity. As schematically shown in Figure 2e, the bipolar output signals of our device can be rectified by using a rectifier bridge circuit before being connected to a capacitor. After the rectification of the output signals, the tactile sensor can be used to charge capacitors (0.22 μ F). As shown in Figure 2e, under a series of pressures, the capacitor accumulates the charges and is charged to about 0.7 V gradually. For the fresh device, the first press leads to a low increased voltage (~ 0.004 V), which means only about 0.88 nC charges are stored in the capacitor. As the number of presses increases, output of the tactile monotonically increases, and the press process causes a relatively large increased voltage (~ 0.06 V) across the capacitor. Thus, about 13.2 nC charges are stored under each press process. These results further confirm our conclusion that the number of the transferred static electrons increases with increasing number of

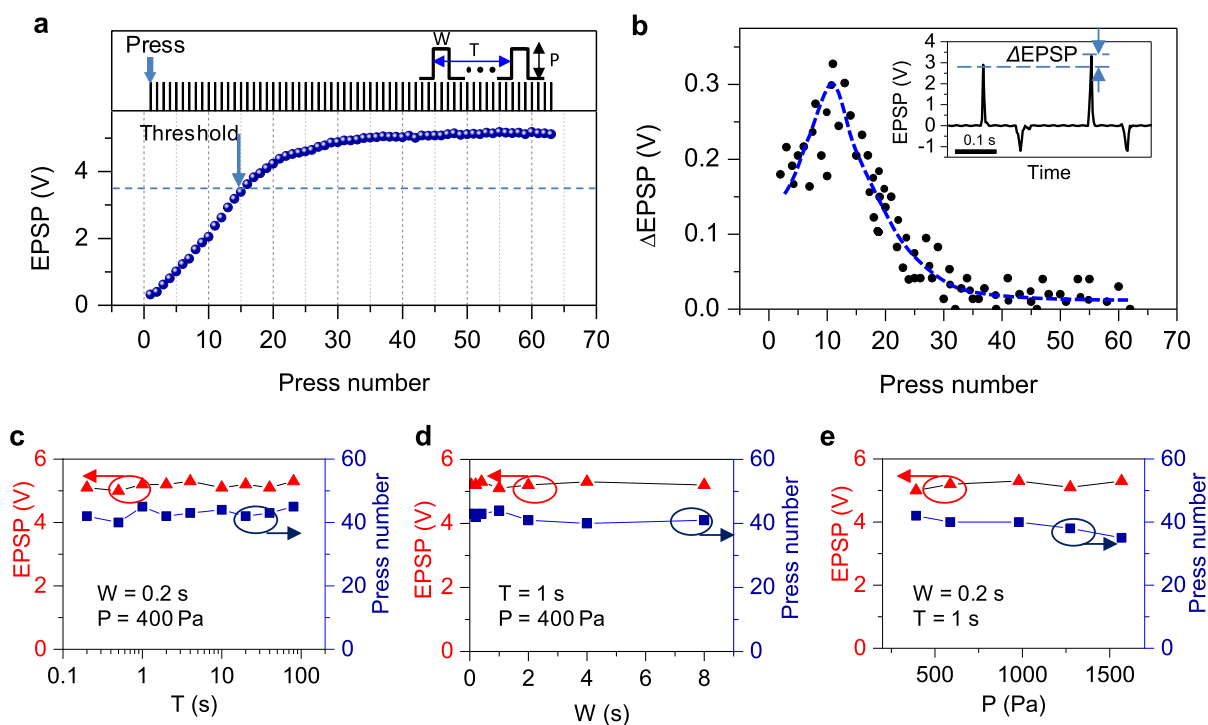


Figure 3. Characterization of learning ability. (a) Output voltage (EPSP) of the intelligent neuromorphic sensor as a function of the number of presses. The external pressure causes the tactile sensor to generate an increasing EPSP. (b) Relationship between Δ EPSP and the press number. The inset shows the details of the Δ EPSP between two EPSP signals. Effects of (c) the time interval, (d) the duration time, and (e) the pressure on the performance of the intelligent neuromorphic sensor.

contact/release cycles. Furthermore, the increasing voltage across the capacitor indicates that our tactile sensor could be further used for driving integrate-and-fire spiking neurons.^{24,28}

Neurobiologically, the learning behaviors of human beings are postulated to be represented by a vastly interconnected neural network in the brain.^{43,44} In particular, an excitatory postsynaptic potential (EPSP) makes the postsynaptic neuron more likely to fire an action potential. For our device, an external pressure causes the tactile sensor to generate increasing voltages, which is similar to the biological EPSP (Figure 3a). Thus, in the following discussion, we will refer to the output potential of our tactile sensor as the EPSP. Similar to the biological postsynaptic potential, the outputs of the intelligent neuromorphic sensor resulting from a single pressure stimulation are too small to reach the threshold (defined as 75% of the final saturated voltage) in the initial state. However, when the tactile sensor receives enough presses, these activities can cause an increased EPSP. When the output is sufficient, an action potential occurs (Figure 3a). For the biological postsynaptic potential, when multiple EPSPs simultaneously occur on a single patch of the postsynaptic membrane, their combined effect is the sum of the individual EPSPs.³⁸ Similar to this biological function, when a series of pressure stimulations is applied to the tactile sensor, the integration of individual changes in the EPSP (Δ EPSP) leads to higher outputs. As shown in inset of Figure 3b, the EPSP difference between the latter and the former pressure stimulations is defined as Δ EPSP. When a series of pressure stimulations is applied, the Δ EPSPs show a positive correlation with the number of presses, and the maximum Δ EPSP can be observed at about the 10th press, after which the Δ EPSP decreases with further increases in the number of presses. The Δ EPSP tends to zero after the \sim 40th press, indicating a

saturated EPSP. Note that the integration of individual presses leads to the final outputs, a process that is similar to that of a biological postsynaptic potential.

The effects of interval time (T), pressure holding time (W), and pressure (P) of the stimulations on the output performances of our intelligent neuromorphic sensor are investigated. The T and W were found to play little role in the output performances (Figure 3c,d). This is because triboelectrification only occurs during the momentary contact between the Al and the PI:rGO layers. Thus, even when pressure is applied with different time intervals and time durations, the total number of transferred electrons is almost the same. As shown in Figure 3e, increasing the pressure cannot increase the final saturated EPSP. However, the maximum number of presses that leads to EPSP saturation decreases slightly with increasing pressure. The reason is that after a sequence of pressure stimulations, the final number of electrons transferred from Al to PI:rGO, which is critical to the final EPSP, is almost the same because the total number of electron traps in the PI:rGO is constant. As a result, increasing the pressure cannot increase the final EPSP. However, increasing the pressure can increase the contact area between the Al and the PI:rGO layers, leading to an increased number of electrons being transferred during each press/release cycle. Thus, the device can reach saturation faster.

From the point of bionics, an interesting behavior, similar to the “learning” behavior of human beings, can be mined in our intelligent neuromorphic sensor. In other words, the experiences with previous pressure stimulations are not ignored; rather they are learned and memorized by the tactile sensor. Thus, the output of a single tactile sensor contains two-dimensional information: (1) the currently generated pulse indicates that an external pressure is presently being applied to

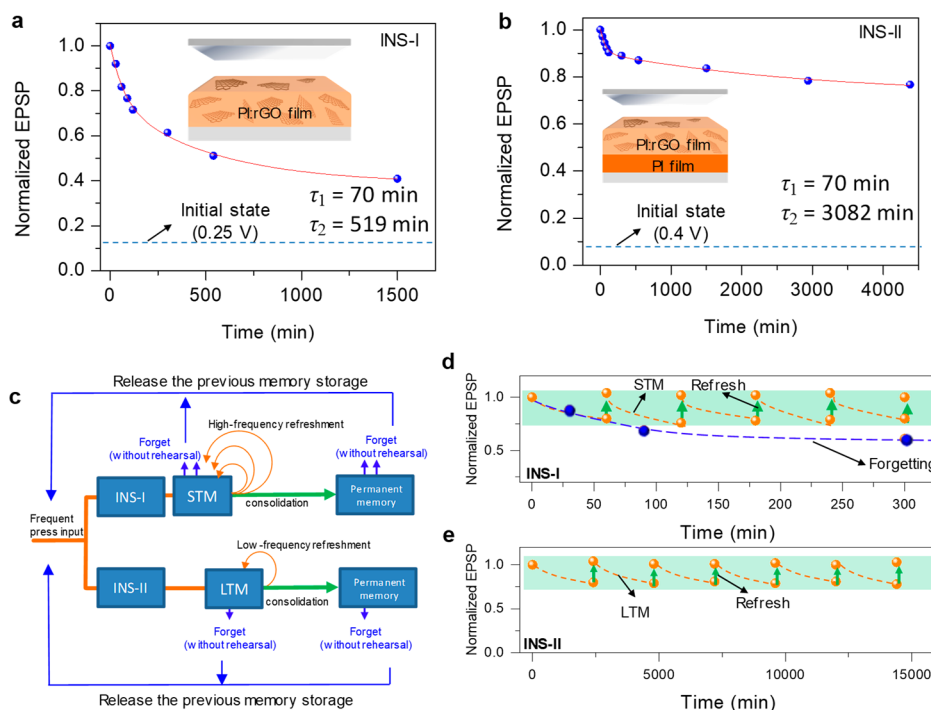


Figure 4. Characterization of the alterable memory performances. (a) Memory retention curve for the INS-I employing a PI:rGO layer as the negative friction layer. Inset is the schematic of INS-I. (b) Memory retention curve for the INS-I employing PI:rGO/PI stacked layer as the negative friction layer. The inset shows a schematic of INS-II. The stacked structure in the friction layer can mediate the retention of memorized information to realize STM and LTM. (c) Schematic of the multistore memory model on the basis of our devices. The measured memorization profiles inspired by the multistore model on the basis of (d) INS-I and (e) INS-II. The yellow dotted lines indicate the decay of the output voltage. The green arrows indicate the refresh process.

the sensor, and (2) the amplitude of the pulse, to some extent, reflects the history of previously applied stimulations.

The key aspect of human memory is information forgetting, which is necessary for human beings to adapt to environments.⁴⁵ To demonstrate the resemblance between the memory of the intelligent neuromorphic sensor and that of the human memory, we first train the tactile sensors to get the saturated output; then the retention output is read by applying a pressure sequence. Here, two kinds of tactile sensors, one that employs a PI:rGO film (INS-I) and the other that employs a PI:rGO/PI film (INS-II) as the negative friction layer, are studied (Figure 4a,b). The decay of the output voltage suggests a surprising similarity to “the forgetting curve” of humans.⁴⁶ Physically, the decay of the output voltage results from the loss of triboelectric charges, and the use of an inserted PI layer can retard that loss process (Figure S7). The reader should note that the applied pressure leads to a slight increase in the output voltage (Δ EPSP). As a result, the measured memory retention curve is slightly different from the real one. However, because the Δ EPSP from each applied press is relatively small (Figure 3b), the small number of applied presses introduced in the retention measurement will not have a large effect on the decay performance of the device.

Quantitatively, a power function, $V = V_1 \exp[-(t/\tau_1)] + V_2 \exp[-(t/\tau_2)]$, is also used to fit the decay curves for our devices.⁴⁷ Here, V is the relaxation function, V_1 and V_2 are the prefactors, t is the time, and τ_1 and τ_2 are the relaxation times, which imply forgetting rates. An abrupt drop is observed in the initial phase ($\tau_1 = 70$ min), followed by a much slower decay ($\tau_2 = 519$ min for the INS-I; $\tau_2 = 3082$ min for the INS-II). The decay trend suggests another surprising similarity to the brief description of human memory; i.e., a rapid initial decline

is usually followed by a long, slow decay.⁴⁸ In biological systems, STM generally lasts from seconds to tens of minutes, and LTM lasts from a few hours to days or weeks, sometimes even to a lifetime.

Based on the different memory retentions, we classify the INS-I and INS-II as the tactile sensors with STM and LTM characteristics, respectively. In other words, the memory for our intelligent neuromorphic sensor can be tuned by modifying the structure of the friction layer. Figure 4c presents a simplified illustration of the multistore memory model on the basis of our intelligent neuromorphic sensor. Frequent pressure stimulations cause both INS-I and INS-II to memorize previously applied stimulations. For INS-I, the memory is lost quickly without repeated stimulations. However, the device can consolidate its memorized information when high-frequency stimulations are applied. For INS-II, the LTM allows it to retain memorized information for a relative long time even without high-frequency refreshment. However, low-frequency refreshment is also necessary for long-term memory. The memory behaviors of the two devices are similar to that of the human memory in that only memories that are of significance (repeated stimulations, training, or study) can be permanently memorized. The different retention properties of the two devices enable cascaded devices to have a multilevel forgetting process and to memorize a rich amount of information, which will be discussed later.

The STM of INS-I lasts tens of minutes, after which a spontaneous decay of the memorization level is observed (orange dashed lines in Figure 4d). Then, 10 pressure stimulations are applied (green arrows in Figure 4d), and the memory can be sustained by rehearsing the same stimulus at high frequency. Interestingly, 10 pressure stimulations are

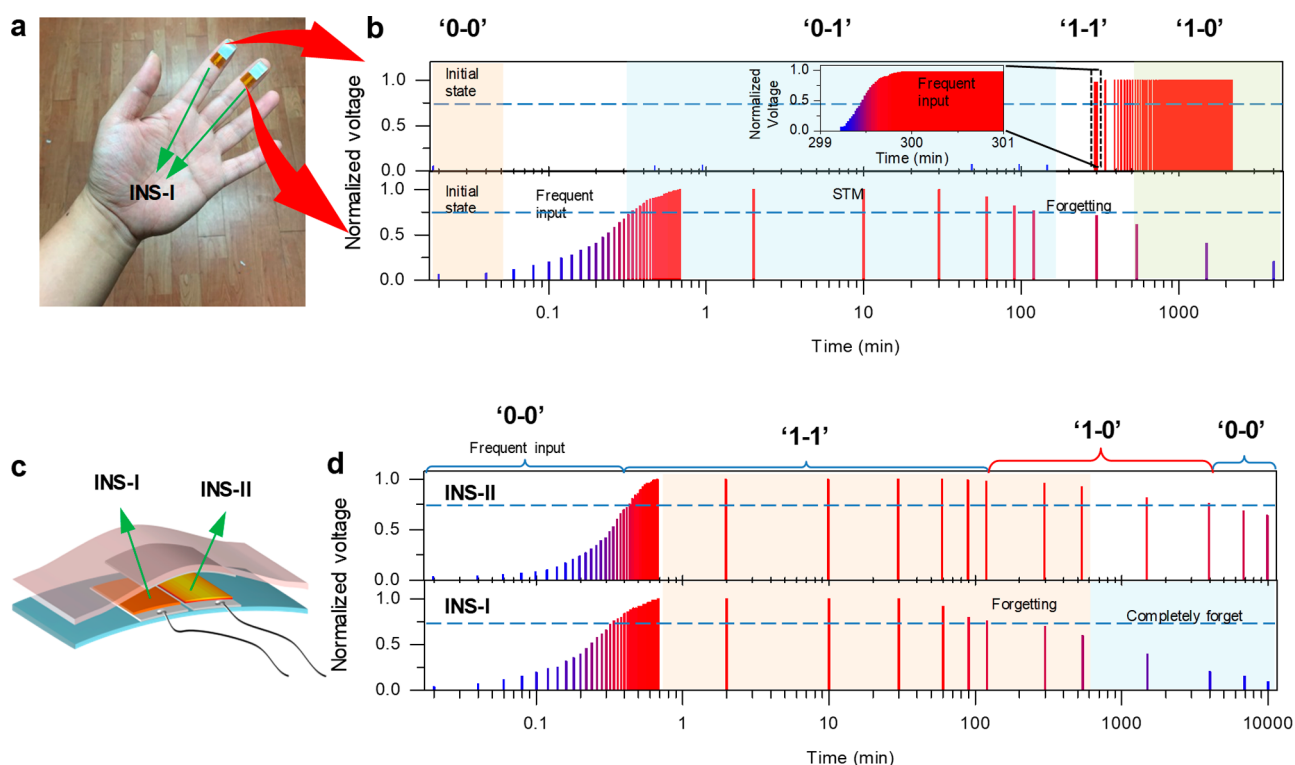


Figure 5. Applications in intelligent fingers. (a) Photograph of two INS-I devices worn, one on each of two fingers. (b) Recorded output signals related to a series of finger actions. (c) Schematic of the tactile sensor integrating INS-I and INS-II into a single device. (d) Recorded output signals related to the fingers' actions. Our intelligent neuromorphic sensor can intelligently record tactile information, such as the current press stimulation, and can retain the history of previous stimulations.

sufficient to obtain the same memorization level after spontaneous decay. This phenomenon is also similar to relearning in the brain, where forgotten information is relearned more quickly than first time information. However, once the refreshing process is stopped, the memorization level will ultimately decay to the initial state (blue dashed lines in Figure 4d), which means that this tactile sensor can release its previously stored memories so as to acquire more frequently accessed or more important information. The LTM from INS-II, despite the presence of forgetting, can be maintained for a much longer period of time without follow-up stimuli. However, relatively low frequency refreshments are necessary if the memory is to become permanent (Figure 4e).

To demonstrate the concrete application, we assembled the devices on fingers to record information related to the actions of the fingers. First, two INS-I were assembled on the middle and the index fingers (Figure 5a). An output pulse lower than the firing threshold is classed as “0” while an output pulse higher than the firing threshold is defined as “1”. In the initial state, both the output pulses under external force (~ 100 mN) are too low to reach the firing threshold, and a signal of “0–0” is recorded (Figure 5b). Thus, we are aware that a pressure has been applied to the fingers currently, which is related to the present stimulations. Furthermore, the signal of “0–0” indicates that the two fingers had not been frequently active, which is related to the previous stimulation history. When the middle finger frequently touches some object, the output from this device increases, and a signal of “0–1” is finally obtained. We can surmise that the middle finger was active more frequently than before (previous stimulation history). When the index finger is also touching some object frequently, the related output also increases, and a signal of “1–1” is obtained.

A motionless middle finger leads to spontaneous decay of the output, so a final signal of “1–0” is recorded.

Because of the different memory retentions, we can integrate INS-I and INS-II into a single device to record a richer amount of action information (Figure 5c and Methods). A single pressure stimulation can produce two voltage outputs, reflecting more information related to the stimulation history. In the initial state, both the outputs under external pressure (~ 100 mN) are low, and a signal of “0–0” is recorded (Figure 5d). Thus, we are aware that this finger was not frequently active. When frequent pressure stimulations are applied to this finger, an output signal of “1–1” is recorded, and this signal will be retained for a long time due to memory retention, which reflects the previous history of frequent actions. However, if frequent pressure stimulations are not applied, the output from INS-I will decrease faster than that from INS-II. As a result, a signal of “1–0” is recorded (Figure 5d). On the basis of the “1–0” signal, we come to know two pieces of information: (1) this finger was active frequently at the very beginning, and (2) this finger has not had any frequent actions in recent times (at least in about 100 min). If no frequent actions are experienced for a long time, the output signal will be reset as “0–0”, which means that the tactile sensor releases its memory storage so as to be able to address a coming action with more frequently accessed or more important information.

The development of a self-powered, intelligent, tactile sensor demonstrates the feasibility of producing an intelligent sensor that can be used to upgrade the function of an electronic tactile sensor from information reception only to information reception and process storage. Furthermore, the idea of functionally integrating a sensor with a neuromorphic system, as was done in this work, can serve as an inspiration for future

development of intelligent sensors able to respond to optical, electrical, chemical, and biological stimulations. Such an intelligent sensor network will have the ability to perceive more information related to its current and previous stimulations and will serve as an interactive interface for an artificial intelligence system. However, the size of the currently constructed, intelligent, tactile sensor is relatively large, and its complexity and integration level are far lower than those required for a biological sensor–nervous system. In the future, further exploration leading to the development of a micrometer-sized, intelligent, tactile sensor and a network with multifunctional integration is necessary.

CONCLUSIONS

In summary, we have demonstrated triboelectric nanogenerator-based intelligent neuromorphic tactile sensors that exhibit self-powered pressure sensing, as well as key features of the neuromorphic system. These sensors are capable of synaptic facilitation and potentiation, memory, and forgetting. In these intelligent, tactile sensors, rGOs embedded in the friction layer acted as electron body traps and played a key role in the neuroplasticity. A temporary increase in the output voltage, as well as a spontaneous decay of that output voltage over time, was observed. The stacked structure in the friction layer was able to mediate the retention time of the information received by the tactile sensors so as to realize STM (relaxation time: 519 min) and LTM (relaxation time: 3082 min). Finally, we showed that the devices could fully conform to the fingers and were able to act as self-powered mechanical sensors with intelligent and tactile sensation and with the ability to retain a rich amount of information related to the current stimulation and to the stimulation history. This highly integrated tactile sensor can serve as a functional element suitable for use in a pressure sensor network of the artificial intelligence system.

METHODS

Preparation of PI:rGO Film. The GO was prepared from purified natural graphite by using the modified Hummers method. PI, from a polyamide acid (PAA) precursor, was prepared by dissolving polyamic acid in dimethylformamide (DMF) and consisted of 287.5 mg of *p*-phenylenediamine (PDA) and 781.25 mg of biphenyltetracarboxylic dianhydride (BPDA) dissolved in 200 mL of DMF solvent. For the preparation of the PAA:GO mixture, 5 mg of GO were added to 10 mL of the PAA precursor, followed by sonication for 1 h. Because GO contains hydroxyl groups on the surfaces and the edges of atomic carbon sheets, the PAA with carboxylic acid groups can readily couple with the GO sheets (Figure S2). The GO sheets were uniformly dispersed in the PAA precursor. The PAA:GO film was deposited on the substrate by using the spin-coating method and was baked at 135 °C for 30 min to evaporate the solvent. This was followed by baking at 400 °C for 2 h to prepare the PI:rGO film (~20 μm).

Fabrication of the Intelligent Neuromorphic Sensors. First, Al foil (1 cm × 1 cm, 10 μm-thick) was prepared for use as an electrode. Then, the PI:rGO film (~20 μm-thick) was fabricated on the surface of the Al foil to form an Al/PI:rGO stacked structure (1 cm × 1 cm), which was attached on PI (Kapton) tape (1.2 cm × 2 cm, 50 μm-thick) to fabricate the bottom component of INS-I. For the bottom component of INS-II, a PI film (~1 μm) was first deposited on the Al foil. The PI:rGO film was attached to the Al/PI substrate to form an Al/PI/PI:rGO film (1 cm × 1 cm). For the bottom component of the intelligent neuromorphic sensor shown in Figure 5c, the Al/PI:rGO stacked structure (1 cm × 1 cm) and the Al/PI/PI:rGO film (1 cm × 1 cm) were attached side-by-side on PI (Kapton) tape (1.2 cm × 3 cm). For the top component of the intelligent neuromorphic sensor, an Al foil (1 cm × 1 cm) was

attached on the oriented polypropylene (OPP) film (1.2 cm × 2 cm, 50 μm-thick) and acted as the positive triboelectric layer. Finally, the Al/OPP stacked film was assembled with the bottom component forming an arch-shaped structure. The chord length of the arch-shaped structure is 1 cm, and the height is about 0.2 cm.

Characterization and Measurement. A scanning electron microscope (SEM, NOVA nanoSEM 450) and an atomic force microscope (AFM, Bruker multimode 8) were used to characterize the GO and the PI:rGO film. For the electrical measurements, the Al electrode was connected to a grounded 10-MΩ resistor, and the output voltages were recorded on an oscilloscope (Tektronix TDS2024C). All the measurements were performed under atmospheric conditions. When the output performance of the intelligent neuromorphic sensors was measured, the devices were placed on a fixed rigid substrate, and a linear motor was used to apply pressure to the device (Figure S8). For the demonstration of the applications of intelligent fingers, the intelligent neuromorphic sensors were assembled on fingers, and the fingers tapped a fixed rigid substrate to apply pressure to the sensors.

ASSOCIATED CONTENT

Supporting Information

The Supporting Information is available free of charge at <https://pubs.acs.org/doi/10.1021/acsnano.9b07165>.

Figures showing AFM image of rGO, schematic of the GO sheet coupled with PAA, working principle of the SE-TENG, durability of the device, schematic illustration of triboelectrification and electron transfer between the Al and the PI film, and measurement setup (PDF)

AUTHOR INFORMATION

Corresponding Authors

*(T.W.K.) E-mail: twk@hanyang.ac.kr.

*(Z.L.W.) E-mail: zhong.wang@mse.gatech.edu.

ORCID

Chaoxing Wu: 0000-0002-1231-2699

Tae Whan Kim: 0000-0001-6899-4986

Chi Zhang: 0000-0002-7511-805X

Zhong Lin Wang: 0000-0002-5530-0380

Author Contributions

T.W.K., Z.L.W., and C.W. conceived the project, C.W. and T.W.K. designed and performed the experiments and collected the data. All authors analyzed and discussed the data. All authors discussed the results and contributed to the writing of the manuscript.

Notes

The authors declare no competing financial interest.

ACKNOWLEDGMENTS

This research was supported by the Basic Science Research Program through the National Research Foundation of Korea (NRF) funded by the Ministry of Education, Science and Technology (2019R1A2B5B03069968). This research was also supported by the NRF funded by Korea government (MSIT) (2018R1A5A7025522).

REFERENCES

- (1) Kim, Y.; Chortos, A.; Xu, W.; Liu, Y.; Oh, J. Y.; Son, D.; Kang, J.; Foudeh, A. M.; Zhu, C.; Lee, Y.; Niu, S.; Liu, J.; Pfattner, R.; Bao, Z.; Lee, T.-W. A Bioinspired Flexible Organic Artificial Afferent Nerve. *Science* **2018**, *360*, 998–1003.

- (2) Hua, Q.; Sun, J.; Liu, H.; Bao, R.; Yu, R.; Zhai, J.; Pan, C.; Wang, Z. L. Skin-Inspired Highly Stretchable and Conformable Matrix Network for Multifunctional Sensing. *Nat. Commun.* **2018**, *9*, 244.
- (3) Kim, D.-H.; Lu, N.; Ma, R.; Kim, Y.-S.; Kim, R.-H.; Wang, S.; Wu, J.; Won, S. M.; Tao, H.; Islam, A.; Yu, K. J.; Kim, T.-I.; Chowdhury, R.; Ying, M.; Xu, L.; Li, M.; Chung, H.-J.; Keum, H.; McCormick, M.; Liu, P.; Zhang, Y.-W.; Omenetto, F. G.; Huang, Y.; Coleman, T.; Rogers, J. A. Epidermal Electronics. *Science* **2011**, *333*, 838–843.
- (4) Guo, S.-Z.; Qiu, K.; Meng, F.; Park, S. H.; McAlpine, M. C. 3D Printed Stretchable Tactile Sensors. *Adv. Mater.* **2017**, *29*, 1701218.
- (5) Wang, S.; Xu, J.; Wang, W.; Wang, G.-J. N.; Rastak, R.; Molina-Lopez, F.; Chung, J. W.; Niu, S.; Feig, V. R.; Lopez, J.; Lei, T.; Kwon, S.-K.; Kim, Y.; Foudeh, A. M.; Ehrlich, A.; Gasperini, A.; Yun, Y.; Murmann, B.; Tok, J. B.-H.; Bao, Z. Skin Electronics from Scalable Fabrication of an Intrinsically Stretchable Transistor Array. *Nature* **2018**, *555*, 83–88.
- (6) Shin, S.-H.; Ji, S.; Choi, S.; Pyo, K.-H.; Wan An, B.; Park, J.; Kim, J.; Kim, J.-Y.; Lee, K.-S.; Kwon, S.-Y.; Heo, J.; Park, B.-G.; Park, J.-U. Integrated Arrays of Air-Dielectric Graphene Transistors as Transparent Active-Matrix Pressure Sensors for Wide Pressure Ranges. *Nat. Commun.* **2017**, *8*, 14950.
- (7) Lei, Z.; Wu, P. A Supramolecular Biomimetic Skin Combining a Wide Spectrum of Mechanical Properties and Multiple Sensory Capabilities. *Nat. Commun.* **2018**, *9*, 1134.
- (8) Wang, X.; Zhang, Y.; Zhang, X.; Huo, Z.; Li, X.; Que, M.; Peng, Z.; Wang, H.; Pan, C. A Highly Stretchable Transparent Self-Powered Triboelectric Tactile Sensor with Metallized Nanofibers for Wearable Electronics. *Adv. Mater.* **2018**, *30*, 1706738.
- (9) Oh, J.; Yang, J. C.; Kim, J.-O.; Park, H.; Kwon, S. Y.; Lee, S.; Sim, J. Y.; Oh, H. W.; Kim, J.; Park, S. Pressure Insensitive Strain Sensor with Facile Solution-Based Process for Tactile Sensing Applications. *ACS Nano* **2018**, *12*, 7546–7553.
- (10) Tee, B. C. K.; Wang, C.; Allen, R.; Bao, Z. N. An Electrically and Mechanically Self-Healing Composite with Pressure- and Flexion-Sensitive Properties for Electronic Skin Applications. *Nat. Nanotechnol.* **2012**, *7*, 825–832.
- (11) He, H. X.; Fu, Y. M.; Zang, W. L.; Wang, Q.; Xing, L. L.; Zhang, Y.; Xue, X. Y. A Flexible Self-Powered T-ZnO/PVDF/Fabric Electronic-Skin with Multi-Functions of Tactile-Perception, Atmosphere-Detection and Self-Clean. *Nano Energy* **2017**, *31*, 37–48.
- (12) Xu, Z.; Wu, C.; Li, F.; Chen, W.; Guo, T.; Kim, T. W. Triboelectric Electronic-Skin Based on Graphene Quantum Dots for Application in Self-Powered, Smart, Artificial Fingers. *Nano Energy* **2018**, *49*, 274–282.
- (13) Lai, Y.-C.; Deng, J.; Niu, S.; Peng, W.; Wu, C.; Liu, R.; Wen, Z.; Wang, Z. L. Electric Eel-Skin-Inspired Mechanically Durable and Super-Stretchable Nanogenerator for Deformable Power Source and Fully Autonomous Conformable Electronic-Skin Applications. *Adv. Mater.* **2016**, *28*, 10024–10032.
- (14) Dhakar, L.; Pitchappa, P.; Tay, F. E. H.; Lee, C. An Intelligent Skin Based Self-Powered Finger Motion Sensor Integrated with Triboelectric Nanogenerator. *Nano Energy* **2016**, *19*, 532–540.
- (15) Wang, X.; Song, W.-Z.; You, M.-H.; Zhang, J.; Yu, M.; Fan, Z.; Ramakrishna, S.; Long, Y.-Z. Bionic Single-Electrode Electronic Skin Unit Based on Piezoelectric Nanogenerator. *ACS Nano* **2018**, *12*, 8588–8596.
- (16) Willis, W. D.; Coggeshall, R. E. *Sensory Mechanisms of the Spinal Cord*; Plenum: New York, 1991.
- (17) Lamprecht, R.; LeDoux, J. Structural Plasticity and Memory. *Nat. Rev. Neurosci.* **2004**, *5*, 45–54.
- (18) Lisman, J.; Cooper, K.; Sehgal, M.; Silva, A. J. Memory Formation Depends on Both Synapse-Specific Modifications of Synaptic Strength and Cell-Specific Increases in Excitability. *Nat. Neurosci.* **2018**, *21*, 309–314.
- (19) Wu, C.; Kim, T. W.; Guo, T.; Li, F.; Lee, D. U.; Yang, J. J. Mimicking Classical Conditioning Based on a Single Flexible Memristor. *Adv. Mater.* **2017**, *29*, 1602890.
- (20) John, R. A.; Liu, F.; Chien, N. A.; Kulkarni, M. R.; Zhu, C.; Fu, Q.; Basu, A.; Liu, Z.; Mathews, N. Synergistic Gating of Electro-Iono-Photoactive 2D Chalcogenide Neuronists: Coexistence of Hebbian and Homeostatic Synaptic Metaplasticity. *Adv. Mater.* **2018**, *30*, 1800220.
- (21) Li, B.; Liu, Y.; Wan, C.; Liu, Z.; Wang, M.; Qi, D.; Yu, J.; Cai, P.; Xiao, M.; Zeng, Y.; Chen, X. Mediating Short-Term Plasticity in an Artificial Memristive Synapse by the Orientation of Silica Mesopores. *Adv. Mater.* **2018**, *30*, 1706395.
- (22) Park, Y.; Lee, J.-S. Artificial Synapses with Short- and Long-Term Memory for Spiking Neural Networks Based on Renewable Materials. *ACS Nano* **2017**, *11*, 8962–8969.
- (23) Shi, Y.; Liang, X.; Yuan, B.; Chen, V.; Li, H.; Hui, F.; Yu, Z.; Yuan, F.; Pop, E.; Wong, H.-S. P.; Lanza, M. Electronic Synapses Made of Layered Two-Dimensional Materials. *Nat. Electron.* **2018**, *1*, 458–465.
- (24) Zhang, X.; Wang, W.; Liu, Q.; Zhao, X.; Wei, J.; Cao, R.; Yao, Z.; Zhu, X.; Zhang, F.; Lv, H.; Long, S.; Liu, M. An Artificial Neuron Based on a Threshold Switching Memristor. *IEEE Electron Device Lett.* **2018**, *39*, 308–311.
- (25) Wu, C.; Kim, T. W.; Choi, H. Y.; Strukov, D. B.; Yang, J. J. Flexible Three-Dimensional Artificial Synapse Networks with Correlated Learning and Trainable Memory Capability. *Nat. Commun.* **2017**, *8*, 752.
- (26) Choi, S.; Tan, S. H.; Li, Z.; Kim, Y.; Choi, C.; Chen, P.-Y.; Yeon, H.; Yu, S.; Kim, J. SiGe Epitaxial Memory for Neuromorphic Computing with Reproducible High Performance Based on Engineered Dislocations. *Nat. Mater.* **2018**, *17*, 335–340.
- (27) Li, C.; Belkin, D.; Li, Y.; Yan, P.; Hu, M.; Ge, N.; Jiang, H.; Montgomery, E.; Lin, P.; Wang, Z.; Song, W.; Strachan, J. P.; Wu, Q.; Williams, R. S.; Yang, J. J.; Xia, Q.; Barnell, M. Efficient and Self-Adaptive *In-Situ* Learning in Multilayer Memristor Neural Networks. *Nat. Commun.* **2018**, *9*, 2385.
- (28) Wang, Z.; Joshi, S.; Savel'ev, S.; Song, W.; Midya, R.; Li, Y.; Rao, M.; Yan, P.; Asapu, S.; Zhuo, Y.; Jiang, H.; Lin, P.; Li, C.; Yoon, J. H.; Upadhyay, N. K.; Zhang, J.; Hu, M.; Strachan, J. P.; Barnell, M.; Wu, Q.; Wu, H.; Williams, R. S.; Xia, Q.; Yang, J. J. Fully Memristive Neural Networks for Pattern Classification with Unsupervised Learning. *Nat. Electron.* **2018**, *1*, 137–145.
- (29) Yoon, J. H.; Wang, Z.; Kim, K. M.; Wu, H.; Ravichandran, V.; Xia, Q.; Hwang, C. S.; Yang, J. J. An Artificial Nociceptor Based on a Diffusive Memristor. *Nat. Commun.* **2018**, *9*, 417.
- (30) Zang, Y.; Shen, H.; Huang, D.; Di, C.-A.; Zhu, D. A Dual-Organic-Transistor-Based Tactile-Perception System with Signal-Processing Functionality. *Adv. Mater.* **2017**, *29*, 1606088.
- (31) Wan, C.; Chen, G.; Fu, Y.; Wang, M.; Matsuhisa, N.; Pan, S.; Pan, L.; Yang, H.; Wan, Q.; Zhu, L.; Chen, X. An Artificial Sensory Neuron with Tactile Perceptual Learning. *Adv. Mater.* **2018**, *30*, 1801291.
- (32) Wang, Z. L. On Maxwell's Displacement Current for Energy and Sensors: The Origin of Nanogenerators. *Mater. Today* **2017**, *20*, 74–82.
- (33) Wang, Z. L. Triboelectric Nanogenerators as New Energy Technology for Self-Powered Systems and as Active Mechanical and Chemical Sensors. *ACS Nano* **2013**, *7*, 9533–9557.
- (34) Bu, T.; Xiao, T.; Yang, Z.; Liu, G.; Fu, X.; Nie, J.; Guo, T.; Pang, Y.; Zhao, J.; Xi, F.; Zhang, C.; Wang, Z. L. Stretchable Triboelectric-Photonic Smart Skin for Tactile and Gesture Sensing. *Adv. Mater.* **2018**, *30*, 1800066.
- (35) Yang, Y.; Zhang, H.; Chen, J.; Jing, Q.; Zhou, Y. S.; Wen, X.; Wang, Z. L. Single-Electrode-Based Sliding Triboelectric Nanogenerator for Self-Powered Displacement Vector Sensor System. *ACS Nano* **2013**, *7*, 7342–7351.
- (36) Hodgkin, A. L.; Huxley, A. F. A Quantitative Description of Membrane Current and Its Application to Conduction and Excitation in Nerve. *J. Physiol.* **1952**, *117*, 500–544.
- (37) Wang, S.; Lin, L.; Wang, Z. L. Nanoscale Triboelectric-Effect-Enabled Energy Conversion for Sustainably Powering Portable Electronics. *Nano Lett.* **2012**, *12*, 6339–6346.

- (38) Wu, C.; Kim, T. W.; Choi, H. Y. Reduced Graphene-Oxide Acting as Electron-Trapping Sites in the Friction Layer for Giant Triboelectric Enhancement. *Nano Energy* **2017**, *32*, 542–550.
- (39) Wu, C.; Kim, T. W.; Park, J. H.; An, H.; Shao, J.; Chen, X.; Wang, Z. L. Enhanced Triboelectric Nanogenerators Based on MoS₂ Monolayer Nanocomposites Acting as Electron-Acceptor Layers. *ACS Nano* **2017**, *11*, 8356–8363.
- (40) Xu, C.; Zi, Y.; Wang, A. C.; Zou, H.; Dai, Y.; He, X.; Wang, P.; Wang, Y.-C.; Feng, P.; Li, D.; Wang, Z. L. On the Electron-Transfer Mechanism in the Contact-Electrification Effect. *Adv. Mater.* **2018**, *30*, 1706790.
- (41) Wu, C.; Park, J. H.; Sung, S.; Koo, B.; Lee, Y. H.; Kim, T. W. Integrable Card-Type Triboelectric Nanogenerators Assembled by Using Less Problematic, Readily Available Materials. *Nano Energy* **2018**, *51*, 383–390.
- (42) Zhou, Y. S.; Wang, S.; Yang, Y.; Zhu, G.; Niu, S.; Lin, Z.-H.; Liu, Y.; Wang, Z. L. Manipulating Nanoscale Contact Electrification by an Applied Electric Field. *Nano Lett.* **2014**, *14*, 1567–1572.
- (43) Cash, S.; Yuste, R. Linear Summation of Excitatory Inputs by CA1 Pyramidal Neurons. *Neuron* **1999**, *22*, 383–394.
- (44) Harrison, J.; Jahr, C. E. Receptor Occupancy Limits Synaptic Depression at Climbing Fiber Synapses. *J. Neurosci.* **2003**, *23*, 377–383.
- (45) Rubin, D. C.; Wenzel, A. E. One Hundred Years of Forgetting: A Quantitative Description of Retention. *Psychol. Rev.* **1996**, *103*, 734–760.
- (46) Ebbinghaus, H. *Memory: A Contribution to Experimental Psychology*; Teacher's College, Columbia University: New York, 1885.
- (47) Phillips, J. C. Stretched Exponential Relaxation in Molecular and Electronic Glasses. *Rep. Prog. Phys.* **1996**, *59*, 1133–1207.
- (48) Wixted, J. T.; Ebbesen, E. B. On the Form of Forgetting. *Psychol. Sci.* **1991**, *2*, 409–415.